Shock-Initiated Fragmentation of n-Dodecane Nano-droplets: A Molecular Dynamics Study

Nikolaos Kateris, Ethan S. Genter, Hai Wang
Department of Mechanical Engineering, Stanford University
Stanford, CA 94305, United States

1 Introduction

Two phase detonation, specifically of liquid fuel droplets in air, is utilized in propulsion and power generation devices, such as pulse and rotating detonation engines [1–4]. Understanding the governing processes in two-phase detonation is necessary for the design and operation of such devices. Specifically, a shock in two-phase detonation impacts liquid fuel droplets, leading to their fragmentation and the mixing of fuel with air. Experimental studies show that upon shock impact, water or hydrocarbon droplets flatten and quickly vaporize along their perimeter; proposed fragmentation mechanisms include Rayleigh-Taylor piercing and shear-induced entrainment [5, 6]. However, the process of shock-droplet interaction is poorly understood due to the lack of spacial and temporal resolution in experimental studies. For this reason, computational fluid dynamics simulations of spray detonations typically treat droplet breakup by a variation of the d^2-law model, which assumes uniform evaporation of a droplet in a hot quiescent gas [7], or semi-empirical liquid stripping models as a part of the droplet evaporation process [8].

In this work, we employ molecular dynamics (MD) to investigate the fragmentation of n-dodecane droplets upon shock impact on a molecular level. The system studied involves droplets 10, 15, and 20 nm in diameter in a Mach 5 nitrogen shock. Upon shock impact, the droplets flatten, lose molecules and subsequently swell and fragment to eventually mix with the surrounding nitrogen in the supercritical phase. The dynamics and energy partitioning are analyzed, showing that droplet fragmentation is a fundamentally non-equilibrium process. The timescale of fragmentation is therefore not able to be predicted by equilibrium-derived laws, such as the d^2-law of evaporation.

2 Methods

Interaction of a Mach 5 shock with droplets 10, 15, and 20 nm in diameter was studied. The pre-shock conditions are 300 K and 7 atm for all three systems, corresponding to Knudsen numbers of 1.00, 0.67, and 0.50, for 10, 15, and 20 nm, respectively. Post-shock conditions at 1500 K and 196 atm correspond to post-shock Knudsen numbers of 0.18, 0.12, and 0.09, respectively, approaching the continuum regime. The reason for the elevated chosen pressure is to achieve Knudsen numbers that are close to the continuum regime, since practical spray detonations operate in that regime.

Molecular dynamics calculations of n-dodecane and nitrogen were run on LAMMPS with a velocity-Verlet integration algorithm [9], using the all-atom L-OPLS force field, which is optimized for long-chain hydrocarbons [10]. To prepare the liquid droplet, a n-dodecane liquid (41,265 molecules) with frozen C-H bonds [11] was simulated. Lennard-Jones and Coulomb interactions were calculated with a cutoff radius of 8.75 Å and 25 Å, respectively. In order to allow the system to relax, energy minimization and a 40 ps NVT simulation were run. An NPT ensemble employing a Nosé-Hoover thermostat and barostat was then used to allow the system to evolve to equilibrium over 1.5 ns. Subsequently, a spherical droplet (of diameter 10, 15, or 20 nm) was cut from the liquid. The liquid droplet was placed in nitrogen gas and the new system was run in an NPT ensemble until a steady state number of adsorbed nitrogen molecules was observed on the surface of the droplet and for at least 100 ps. Simultaneous to the creation of the liquid droplet, a large box was filled with nitrogen gas and relaxed for 40 ps in the same fashion as the n-dodecane liquid until the desired pressure was established. Box lengths for the 10, 15, and 20 nm droplets were 2 μm, 2.5 μm, and 5 μm, respectively, with corresponding box widths of 115 nm × 115 nm, 120 nm × 120 nm, and 125 nm × 125 nm. The box widths are designed to allow at least 5 mean free paths of pre-shock gas on each side of the droplet. Following equilibration, a reflective piston boundary condition was applied at one face of the box with a reflective wall at the other end, with periodic boundary conditions in the non-length-wise directions. The piston was then advanced at $U_{piston} = 0.0142$ Å/fs to initiate a Mach 5 shock. Once a steady shock speed was observed, the simulation was paused and a spherical hole, slightly larger than the droplet itself, was cut in the quiescent gas in front of the shock. The liquid droplet and some of its surrounding nitrogen gas prepared earlier were placed ahead of the shock, as shown in Fig. 1a, and the virtual piston was allowed to continue advancing the shock, causing it to impact the droplet at a later time.

3   Results and Discussion

MD allows a direct observation of detailed dynamics through tracking the atomic coordinates of atoms belonging to n-dodecane or the nitrogen gas. As the piston of Fig. 1a moves at a given supersonic speed, the shock impacts the droplet, shown in the first panel of Fig. 1b for a 10 nm droplet. Subsequently, The droplet first flattens in the first 20 ps due to the fast moving compressed gas impacting the quiescent droplet and delivering a strong impulse. The droplet subsequently undergoes surface ablation and starts to lose n-dodecane molecules around its perimeter. After 140 ps the main body of the droplet swells, undergoing bulk expansion or microexplosions, which are evident as voids in the zoomed in view in Fig. 1b. This process is fundamentally different from surface evaporation or surface stripping, as the whole volume of liquid phase expands simultaneously, leading to fragmentation. Eventually, a liquid phase is no longer discernible and all n-dodecane molecules exist in small clusters or as lone molecules mixed with the surrounding nitrogen, resembling the molecular behavior of a supercritical fluid (note that the critical point for n-dodecane is 658 K, 17.9 atm [?]), both of which are lower than the post-shock The same behavior is observed for larger droplets at a relatively slower rate.

Figure 1c shows the temperature of n-dodecane, as well as the center-of-mass position and velocity of the n-dodecane droplet as a function of time. It can be seen that temperature starts increasing approximately linearly with time, until it levels off at a value close to the temperature of the compressed nitrogen gas. Upon shock impact, the droplet also experiences a strong acceleration due to the drag by the post-shock gas, with its velocity rapidly increasing and reaching the velocity of the post-shock gas. Importantly, due to the flattening and swelling of the droplet, the velocity increase is more rapid than what would be predicted by the Stokes drag under the limiting, no-slip limit.

The energy increase of the droplet manifests in its rapid heating and acceleration and can be analyzed in terms of kinetic and potential energy components. Kinetic and potential energy are further partitioned
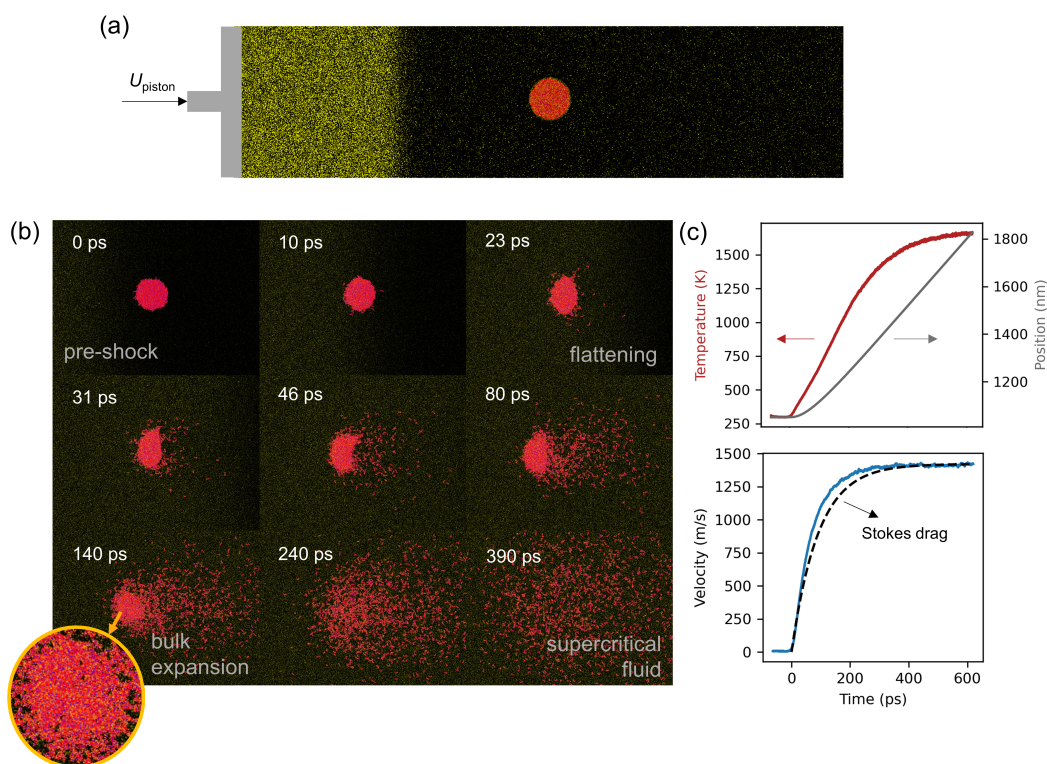
Figure 1: (a) Schematic (not to scale) of a nitrogen (yellow) shock being driven by the reflective piston, before impact with the n-dodecane (red) droplet. (b) Snapshots at different times after shock impact, showing droplet behavior, including flattening, initial surface molecule escape, and bulk expansion and fragmentation. (c) n-dodecane temperature and droplet center of mass position and velocity as a function of time.

into different degrees of freedom of motion and types of intermolecular interactions, respectively. Figure 2a shows the kinetic and potential energy of the droplet and their constituent components. The total kinetic energy of the droplet involves its bulk motion, which if subtracted, yields the kinetic energy of the droplet in the droplet frame of reference. The kinetic energy in the droplet frame is approximately equal to the droplet potential energy (due to the virial theorem) and arises due to the translational, rotational, and vibrational degrees of freedom of n-dodecane molecules. As shown in Fig. 2a, the translational kinetic energy is only a small fraction of the droplet kinetic energy, due to polyatomic n-dodecane molecules with frozen C-H bonds having 3 translational degrees of freedom and 85 internal degrees of freedom.

Normalizing the components of kinetic energy by the energy contribution of total, translational, and internal degrees of freedom allows the assignment of an overall, translational, and internal temperature to the droplet, as presented in the lower panel of Fig. 2a. Notably, the droplet is translationally overheated, while internal temperature lags behind. That is, n-dodecane is not in thermodynamic equilibrium until some $400\,\mathrm{ps}$ after shock impact, when translational and internal temperatures are equal to one another. The translational overheating is attributed to the liquid oscillation induced by the shock to the droplet, which sets molecules in motion relative to the droplet's center of mass.

The potential energy of the droplet can in turn be decomposed into a surface energy contribution and a phase change contribution. Evaluating changes in surface energy involves the evaluation of changes in surface area, as well as the change in surface tension due to droplet heating. Figure 2b shows the initial
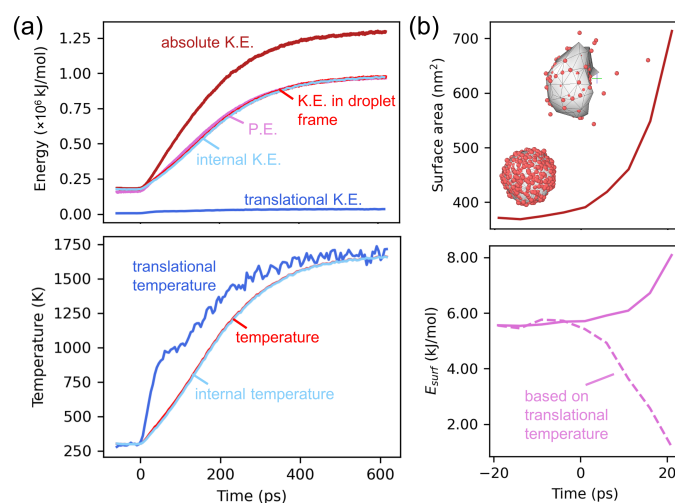
Figure 2: (a) The partitioning of energy and temperature of the droplet. Potential energy is represented in pink. The overall kinetic energy (dark red) is translated into kinetic energy in the droplet frame (red), which corresponds to the droplet temperature. This can be further decomposed into a translational contribution (dark blue) and an internal contribution (light blue). (b) The increase in surface area of the droplet and the change in surface energy, shortly after shock impact.

increase of the droplet surface area, calculated for a smoothed surface mesh encompassing most n-dodecane molecules before major vaporization events. The increase in temperature leads to a decrease in surface tension, which is amplified if the surface tension is calculated based on translational temperature, since internal degrees of freedom will not strongly affect intermolecular interactions. The lower panel of Figure 2b shows the change in surface energy, which is the combined effect of the increase in surface area and the decrease in surface tension. Surface energy increases if surface tension varies with overall temperature and decreases for the calculation based on translational temperature, but in both cases the change in surface energy is negligible. It can thus be concluded that all change in potential energy is associated with overcoming intermolecular interactions, and thus droplet fragmentation and phase change.

The breaking of intermolecular "bonds" is the basis of a cluster analysis to quantify the fragmentation timescale, presented in Fig. 3. Grouping molecules whose centers of mass are at a distance smaller than a cutoff distance r_{cutoff} in the same cluster, as illustrated in Fig. 3a, and tracking the number of molecules in the largest cluster in the system, allows the identification of the timescale when phase change is complete, that is, when the number of molecules in the largest cluster reaches a steady state. The choice of r_{cutoff}, however, affects the result of this analysis, thus phase change requires more careful consideration.

The phase of the droplet can thus be examined by calculating the radial distribution function of n-dodecane molecules, shown in Fig. 3b. Initially the droplet is in the liquid phase and exhibits a short nearest neighbor distance and clear first and second solvation shell peaks. After $190\,\mathrm{ps}$ the radial distribution function exhibits a longer nearest neighbor distance and no solvation shell characteristics, indicating that the droplet is no longer in the liquid phase, but resembles a volume of gas or a group of supercritical gas-like clusters. The shape of the radial distribution function does not vary with time, but the distribution flattens as the gas expands and mixes with the surrounding nitrogen.

Employing different values of r_{cutoff} and calculating the droplet fragmentation timescale leads to the conclusion that $r_{\mathrm{cutoff}} = 8.75\,\text{Å}$, where $8.75\,\text{Å}$ is the attractive van der Waals cutoff distance, providing
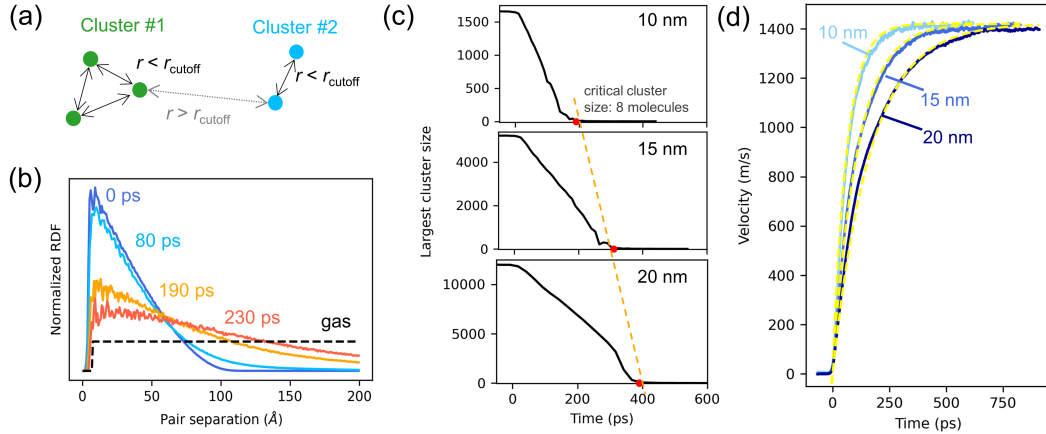
Figure 3: (a) Schematic representing cluster assignment, with circles corresponding to centers of mass of n-dodecane molecules. (b) Radial distribution function of a 10 nm droplet at different times after shock impact. (c) The time evolution of the number of molecules in the largest n-dodecane cluster in the system. (d) Velocity of 10, 15, and 20 nm droplets and predicted velocity (in yellow), based on effective diameter slip-corrected drag.

a result that is consistent with the radial distribution function observations. The cluster analysis is applied to droplets of 10, 15, and 20 nm in size and the results are shown in Fig. 3c. The timescale after which the largest cluster no longer changes in size and all n-dodecane behaves a supercritical gas is equal to 190, 310, and 390 ps for 10, 15, and 20 nm, respectively, indicating a linear relationship with size, rather than the d^2 relationship dictated by the d^2-law of evaporation.

A new theory describing droplet dynamics behind shock needs to consider both momentum and energy deposition, as the two are intimately coupled. Acceleration and fragmentation occur at similar timescales, as concluded from Figs. 1c and 3c, and a model for momentum gain is presented here. The drag of the droplet due to the fast-moving post-shock gas is amplified by the flattening of its shape, but weakened due to slip on the droplet surface, as the droplet is in the transition or slip flow regime. It should be noted that droplet flattening occurs due to impact from the fast moving gas and not due to the onset of a liquid droplet vibrational mode, since the flattening timescale is two orders of magnitude smaller than the droplet vibrational frequency ($\mathcal{O}(10\,\mathrm{ps})$ vs $\mathcal{O}(1\,\mathrm{ns})$). The two competing effects are captured by the effective diameter and the Cunningham slip correction [12] in the following drag expression:

$$D = -\frac{3\pi\mu d_{\mathrm{eff}}V_{\mathrm{rel}}}{1 + 2Kn(A_1 + A_2 e^{-A_3/Kn})}.$$

With an appropriate model for d_{eff}, the above expression can recreate the measured velocity evolution of the droplets impacted by a shock. Assuming a power relationship between d_{eff} and d, due to the approximately volume-conserving flattening observed, the expression $d_{\mathrm{eff}} = 962\,\mathrm{nm}^{-0.35}d^{1.35}$ arises, accurately recreating MD data.

4   Conclusions

Molecular dynamics simulations for the interaction of Mach 5 shocks with droplets of 10, 15, and 25 nm in diameter examine the fragmentation dynamics of droplets in post-shock conditions that approach the continuum regime. Droplets flatten, swell, and fragment in a non-equilibrium process characterized by translational overheating. Shock impact enhances acceleration and energy deposition, leading to rapid

droplet fragmentation, which dominates phase transition. The fragmentation time scale is linear with droplet size, therefore evaporation laws, such as the d^2-law of evaporation are not applicable to two phase detonation, where shocks rapidly deposit energy to fuel droplets in a rapid non-equilibrium process. A theory for momentum and energy deposition to the droplet, ultimately leading to its fragmentation, is challenging due to the coupled nature of the phenomena, but is necessary for the accurate modeling of spray detonation.

5 Acknowledgement

References

[1] T. Bussing and G. Pappas, "An introduction to pulse detonation engines," in *32nd Aerospace Sciences Meeting and Exhibit*, p. 263, 1994.

[2] J. Kindracki, "Experimental research on rotating detonation in liquid fuel–gaseous air mixtures," *Aerosp. Sci. Technol.*, vol. 43, pp. 445–453, 2015.

[3] R. Zhou, D. Wu, and J. Wang, "Progress of continuously rotating detonation engines," *Chinese J. Aeronaut.*, vol. 29, no. 1, pp. 15–29, 2016.

[4] J.-M. Li, P.-H. Chang, L. Li, Y. Yang, C. J. Teo, and B. C. Khoo, "Investigation of injection strategy for liquid-fuel rotating detonation engine," in *2018 AIAA Aerospace Sciences Meeting*, p. 0403, 2018.

[5] R. Bar-Or, M. Sichel, and J. Nicholls, "The reaction zone structure of cylindrical detonations in monodisperse sprays," in *Symp. (Int.) on Combust.*, vol. 19, pp. 665–673, 1982.

[6] S. Sharma, A. P. Singh, S. S. Rao, A. Kumar, and S. Basu, "Shock induced aerobreakup of a droplet," *J. Fluid Mech.*, vol. 929, 2021.

[7] I. Langmuir, "The evaporation of small spheres," *Phys. Rev.*, vol. 12, no. 5, p. 368, 1918.

[8] J. A. Nicholls and A. Ranger, "Aerodynamic shattering of liquid drops.," *AIAA J.*, vol. 7, no. 2, pp. 285–290, 1969.

[9] A. P. Thompson, H. M. Aktulga, R. Berger, D. S. Bolintineanu, W. M. Brown, P. S. Crozier, P. J. in't Veld, A. Kohlmeyer, S. G. Moore, T. D. Nguyen, *et al.*, "LAMMPS-a flexible simulation tool for particle-based materials modeling at the atomic, meso, and continuum scales," *Comput. Phys. Commun.*, vol. 271, p. 108171, 2022.

[10] S. W. Siu, K. Pluhackova, and R. A. Böckmann, "Optimization of the OPLS-AA force field for long hydrocarbons," *J. Chem. Theory Comput.*, vol. 8, no. 4, pp. 1459–1470, 2012.

[11] H. C. Andersen, "Rattle: A "velocity" version of the shake algorithm for molecular dynamics calculations," *J. Comput. Phys.*, vol. 52, no. 1, pp. 24–34, 1983.

[12] E. Cunningham, "On the velocity of steady fall of spherical particles through fluid medium," *Proc. R. soc. Lond. Ser. A-Contain. Pap. Math. Phys. Character*, vol. 83, no. 563, pp. 357–365, 1910.